THE JOURNAL OF PHYSICAL CHEMISTRY A

 VOLUME 113, NUMBER 37, SEPTEMBER 17, 2009

ARTICLES

Infrared Spectroscopy and Quantum Chemical Calculations of OH-$(H_2O)_n$ Complexes

Kazuhide Tsuji*,† and Kazuhiko Shibuya*,‡

Gunma National College of Technology, Maebashi 371-8530, Japan, and Department of Chemistry, Graduate School of Science and Engineering, Tokyo Institute of Technology, Tokyo 152-8551, Japan

Received: April 21, 2009; Revised Manuscript Received: August 4, 2009

Infrared spectra of OH-$(H_2O)_n$ ($n = 1, 2$) isolated in solid Ne were measured by FT-IR spectroscopy. Complexes of OH-$(H_2O)_n$ were prepared by vacuum ultraviolet (VUV) photolysis of water clusters, and the OH radical stretch and HOH bending vibrations of OH-H_2O and OH-$(H_2O)_2$ complexes were identified with the aid of quantum chemical calculations. Observation of the recombination reaction OH-H_2O + H → $(H_2O)_2$ under dark conditions provides undisputed evidence for our spectroscopic assignment. Quantum chemical calculations predict the cyclic structure to be the most stable for OH-$(H_2O)_2$ and OH-$(H_2O)_3$. The strength of the hydrogen bond within OH-$(H_2O)_n$ depends on cluster size.

Introduction

The OH radical plays a key role in physical, chemical, and biological sciences. It is an important chemical intermediate in gas-phase reactions such as combustion and atmospheric chemistry, and a central mediator in aqueous radiation processes and sonochemical reactions. However, fundamental questions remain concerning issues such as hydration in the liquid phase[1,2] and mass accommodation at the gas−liquid interface.[3,4] To better understand these issues, we need more information on the hydrated hydroxyl radical OH-$(H_2O)_n$.

Recently, OH-H_2O complexes were experimentally investigated by matrix-isolation IR spectroscopy in solid Ar matrices[5−7] and by microwave spectroscopy in the gas phase.[8] High-level ab initio calculations using technique such as QCISD and CCSD(T) were also reported.[6,8] All calculations reported to date suggest that the global minimum of the OH-H_2O interaction potential is for an OH···OH_2 type structure, which is supported by microwave spectroscopy data.[8] Matrix isolation spectroscopy has provided detailed information on the OH radical stretching vibration of OH-H_2O in solid Ar and on site splitting of the IR band.[5−7]

In this study, we report the first identification of an OH-$(H_2O)_n$ ($n = 1, 2$) complex, isolated in a Ne matrix, by Fourier-transform IR (FT-IR) spectroscopy. One advantage of solid Ne as a cryogenic medium is that perturbation of dopant molecules is negligibly weak. IR frequencies measured in the Ne matrix are thus expected to be close to those measured in the gas phase. Moreover, the small interaction between molecule and Ne results in simple IR spectra free from complicated splittings due to matrix site effects. We present the rigorous spectroscopic assignment for the OH-H_2O band and the first report of spectroscopic information on OH-$(H_2O)_2$. These assignments are supported by quantum chemical calculations.

Experimental and Computational Methods

The experimental apparatus was essentially the same as that reported elsewhere.[9] A CsI plate cooled to 5 K with a closed-cycle helium refrigerator (Iwatani CW303) served as a substrate

* Corresponding authors. E-mail: ktsuji@nat.gunma-ct.ac.jp (K.T.); kshibuya@chem.titech.ac.jp (K S.). Fax: +81-27-254-9281.
† Gunma National College of Technology.
‡ Tokyo Institute of Technology.

10.1021/jp903648z CCC: $40.75
Published on Web 08/18/2009

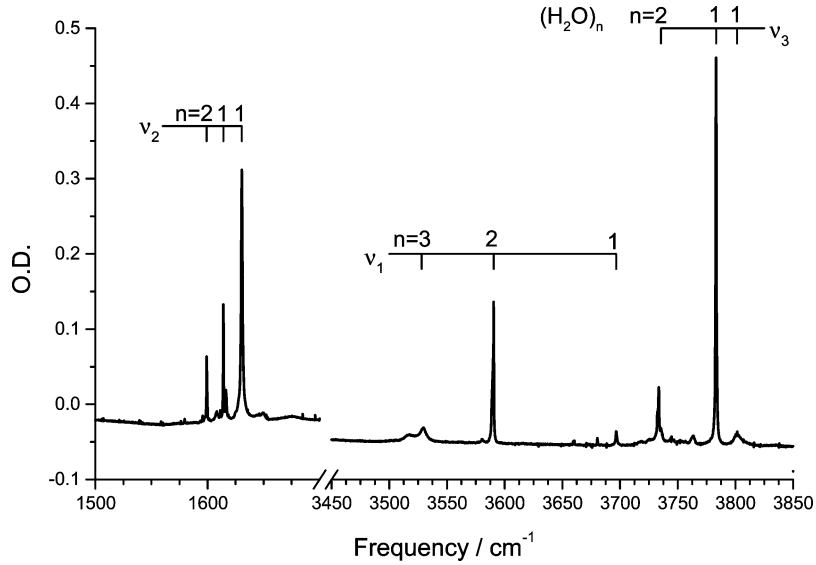

Figure 1. IR spectrum of $(H_2O)_n$ isolated in a Ne matrix in the H_2O bending and OH stretching regions.

TABLE 1: IR Bands of $(H_2O)_n$ Isolated in Solid Ne

frequency (cm^{-1})	assignment
1599.2	$(H_2O)_2$, H-acceptor, ν_2
1614.1	H_2O, ν_2 $1_{0,1} \rightarrow 1_{1,0}$
1616.4	$(H_2O)_2$, H-donor, ν_2
1630.5	H_2O, ν_2 $0_{0,0} \rightarrow 1_{1,1}$
1649.5	H_2O, ν_2 $1_{0,1} \rightarrow 2_{1,2}$
3382	$(H_2O)_4$
3528	$(H_2O)_3$
3590.5	$(H_2O)_2$, H-donor, ν_1
3680.4	$(H_2O)_2$, H-acceptor, ν_1
3696.7	H_2O, ν_1 $0_{0,0} \rightarrow 1_{1,1}$
3733.6	$(H_2O)_2$, H-donor, ν_3
3735.5	H_2O, ν_3 $1_{0,1} \rightarrow 0_{0,0}$
3763.3	
3783.2	H_2O, ν_3 $0_{0,0} \rightarrow 1_{0,1}$
3801.5	H_2O, ν_3 $1_{0,1} \rightarrow 2_{0,2}$

TABLE 2: IR Bands of VUV-Photolysis Products in Solid Ne

frequency (cm^{-1})	assignment
1598.6	OH-(H_2O), HOH bending
3365.2	OH-$(H_2O)_2$, OH radical stretch
3382	$(H_2O)_4$
3472.5	OH-H_2O, OH radical stretch
3528	$(H_2O)_3$
3566	OH

for a cold matrix sample. Gaseous mixtures of H_2O/Ne (typical dilution ratio 1:3000) were deposited over several hours. IR absorption spectra were measured with an FT-IR spectrometer (JEOL SPX200) equipped with a mercury cadmium telluride (MCT) detector cooled to 77 K. The irradiation source was a lamp unit of a vacuum ultraviolet (VUV) light around 172 nm (Ushio, UER20-172A). To avoid IR absorption of water vapor and CO_2 gas in ambient air, the spectrometer's optical system was purged with nitrogen from a nitrogen gas generator (Iwatani). Typically, 100 scans were accumulated with a spectral resolution of 0.25 cm^{-1}.

Equilibrium structure, energy, vibrational frequency, and IR intensity were calculated with a Gaussian 03 program.[10] Geometry optimizations and vibrational frequency calculations for OH-$(H_2O)_n$ ($n = 1-3$) and $(H_2O)_n$ ($n = 1-4$) were performed using density functional theories (DFTs) B3LYP and B98, and ab initio calculations of second-order Møller−Plesset

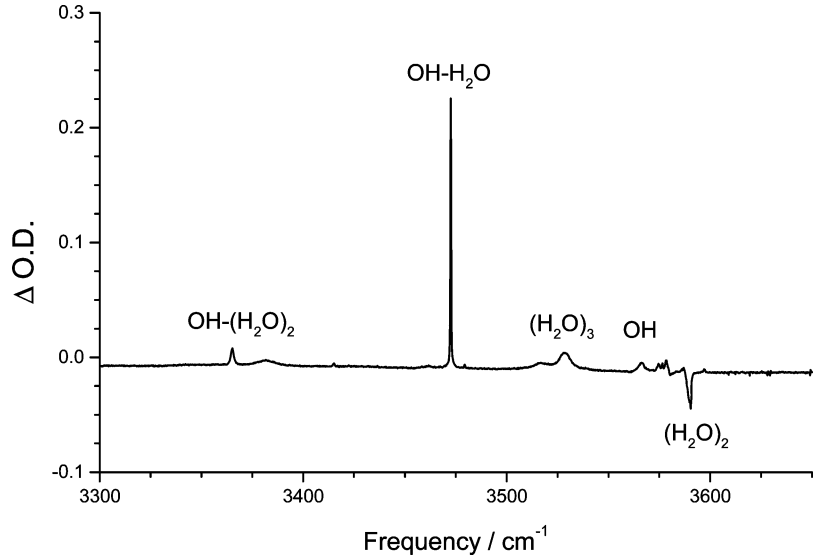

Figure 2. Difference IR spectrum for VUV photolysis in the OH stretching region. The bands due to $(H_2O)_n$ decrease.

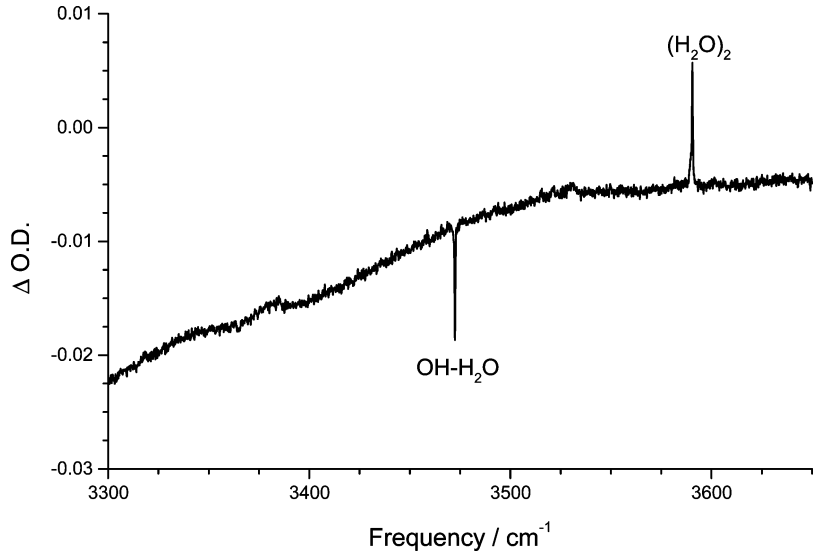

Figure 3. Difference IR spectrum for dark reaction in the OH stretching region.

perturbation theory MP2 and fourth-order Møller−Plesset perturbation theory MP4(SDQ) with the basis sets aug-cc-pVDZ, and aug-cc-pVTZ. Basis set superposition error (BSSE) was minimized with the counterpoise corrections of Boys and Bernardi.[11] A chemical graphic program, Facio, was used to plot 3D molecular structures.[12,13]

Results and Discussion

Matrix-Isolation Spectra. Figure 1 shows the HOH bending and OH stretching regions of an IR spectrum recorded for the cryogenic matrix of a water/Ne-gas mixture. In addition to the rovibrational lines of H_2O monomer, several bands due to H_2O clusters $(H_2O)_n$ ($n = 2, 3$) are clearly identified.[14,15] Weak peaks due to $(H_2O)_4$ are also assigned based on a gas phase study[16] and matrix isolation studies in other media.[17−20] Table 1 lists the band positions and assignments.

Figure 2 shows a difference spectrum recorded after the matrix was irradiated with VUV light. The spectrum was obtained by subtracting the spectrum measured for the deposited matrix (Figure 1) from that measured after irradiation. Positive and negative peaks correspond to growth of photoproducts and depletion of reactants, respectively. Table 2 lists the frequencies of the observed photoproduct bands. The weak 3566 cm^{-1} band is assigned to the matrix-isolated OH radical.[6] Several bands are observed to its lower-frequency side. The most intense band is at 3472.5 cm^{-1}, which is red-shifted by 94 cm^{-1} from 3566 cm^{-1}. In solid Ar, the OH radical stretch of OH-H_2O is reported to be at 3452.2 cm^{-1}, which represents a red shift of 97 cm^{-1} from the OH monomer band.[5,6] The shift of 94 cm^{-1} measured in solid Ne is close to the reported shift of 97 cm^{-1} in solid Ar suggesting that the 3472.5 cm^{-1} band can be attributed to OH-H_2O (more rigorous discussion of band assignment follows).

A band at 3365.2 cm^{-1} in the figure is red-shifted by 201 cm^{-1} from the OH monomer band, almost twice as far as the 94 cm^{-1} shift for OH-H_2O. This double shift suggests that the 3365.2 cm^{-1} band may be due to the OH radical stretch of the doubly hydrogen-bonded OH radical in OH-$(H_2O)_n$, HOH···OH···OH_2, although the number of water molecules n and the structure of the cluster are uncertain at this moment.

We studied the occurrence of dark reactions by recording an IR spectrum after the irradiated matrix was left in the dark for several hours. Figure 3 shows the difference spectrum, obtained by taking the difference between spectra recorded before and after dark storage. The positive bands are due to dark reaction products; the negative bands are due to reactants. The figure clearly indicates the occurrence of dark reactions. The photoproduct band at 3472.5 cm^{-1}, tentatively assigned to OH-H_2O, is negative, and the $(H_2O)_2$ band at 3590.5 cm^{-1} is positive, consistent with dark reaction from OH-H_2O to $(H_2O)_2$. During VUV photolysis of H_2O/Ne matrices, water dissociates into OH radicals and H atoms. H atoms are known to diffuse in solid rare gas,[21,22] until they encounter other atoms, molecules, or radicals, and are expected to live long in solid rare gas, with which they do not react. In the present solid Ne system, H atoms diffuse until they encounter OH radicals to form H_2O or H atoms to form H_2. Therefore, observation of simultaneous OH-H_2O consumption and $(H_2O)_2$ generation in the dark provides additional evidence that the 3472.5 cm^{-1} band is due to OH-H_2O.

It is interesting to compare the OH radical stretching band intensities of OH monomer and OH-H_2O. The OH-H_2O band at 3472.5 cm^{-1} is roughly 30−40 times more intense than the OH monomer band at 3566 cm^{-1} (Figure 2). However, the band intensities of the corresponding parent molecules $(H_2O)_2$ and H_2O are comparable; for example, the $(H_2O)_2$ band at 3590.5 cm^{-1} is roughly $^1/_3$ times the intensity of the H_2O band at 3783.2 cm^{-1} (Figure 1). A consequence of the low H_2O concentration in Ne gas (H_2O/Ne = 1/3000) in the present experiment is that the solid Ne contains H_2O in preference to $(H_2O)_2$, consistent with the comparable IR intensities for the H_2O and $(H_2O)_2$ bands. However, it is difficult to understand why the OH-H_2O band at 3472.5 cm^{-1} is more intense than the OH monomer band at 3566 cm^{-1}. Possible explanations are that (1) the quantum yield is higher for VUV photodissociation of $(H_2O)_2$ into OH-H_2O than for VUV photodissociation of H_2O into OH radical; and/or (2) the IR absorption coefficient for the OH radical stretch is enhanced by complexation with H_2O. This unusual intensity ratio is discussed later.

The lower trace of Figure 4 shows the difference IR spectrum upon VUV photolysis in the H_2O bending region. The frequency of the observed photoproduct band is also listed in Table 2. Unlike for OH stretching, the H_2O bending band at 1598.6 cm^{-1} due to a photoproduct overlaps with the 1599.2 cm^{-1} band due to the H-accepting moiety of $(H_2O)_2$.[14] Depletion of the parent $(H_2O)_2$ band is accompanied by growth of the photoproduct band, and the difference spectrum shows the differential

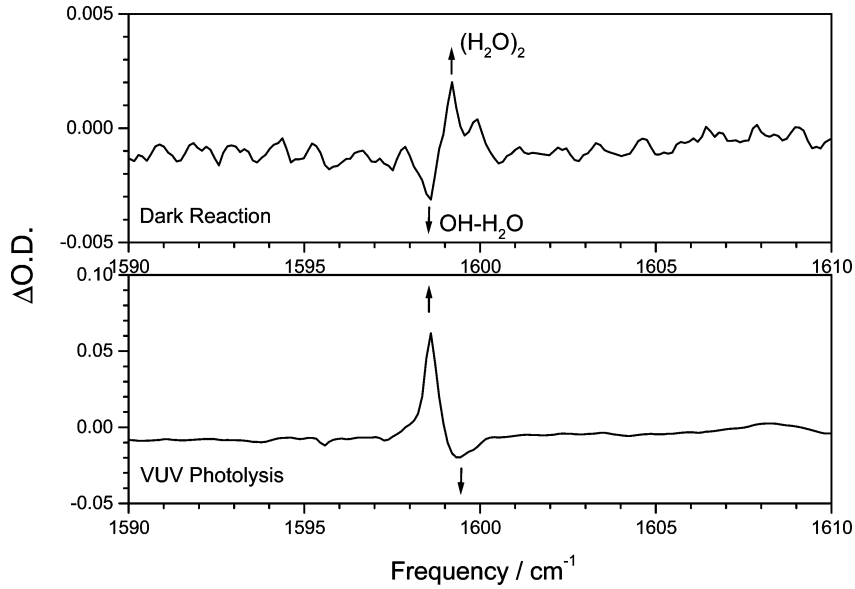

Figure 4. Difference IR spectra for VUV photolysis (lower trace) and dark reaction (upper trace) in the H_2O bending region.

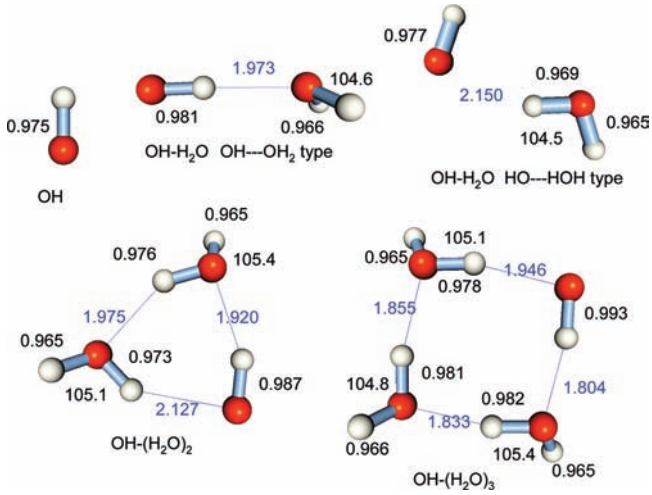

Figure 5. Optimized structures of OH-$(H_2O)_n$ at the MP2/aug-cc-pVDZ level theory together with the molecular parameters (bond lengths in Å, angles in deg).

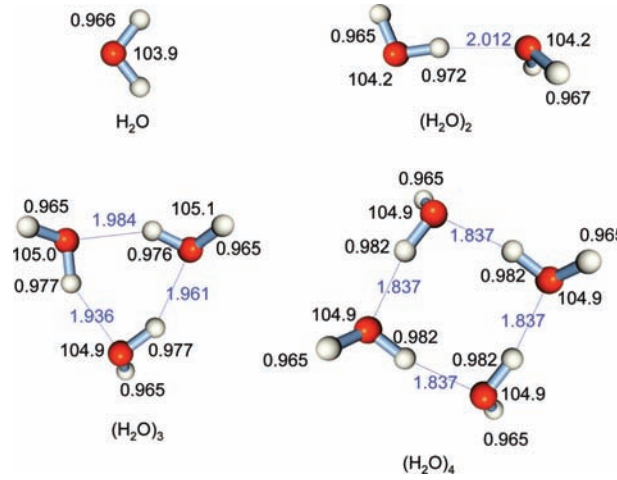

Figure 6. Optimized structures of $(H_2O)_n$ at the MP2/aug-cc-pVDZ level of theory together with the molecular parameters (bond lengths in Å, angles in deg).

waveform. Recovery of $(H_2O)_2$ in the dark creates an opposite-phase differential waveform shown in the upper trace of the figure, indicating the occurrence of bidirectional pathways: (1) the photolysis of $(H_2O)_2$ to produce OH-H_2O, and (2) dark reaction of OH-H_2O and H atom to reproduce $(H_2O)_2$. Significantly, the H_2O bending vibration of the photoproduct is similar to that within the H-accepting moiety of the H_2O dimer; that is, the OH radical within the complex is hydrogen-bonded to the O atom of H_2O.

These spectroscopic results show that the stretching frequency of the OH radical is strongly influenced by water-complex formation, while the H_2O bending frequency of OH-H_2O is almost identical to that of the H-accepting moiety of $(H_2O)_2$. These observations strongly suggest that the OH-H_2O complex has an OH···OH_2 type structure, where the OH radical acts as hydrogen donor and the H_2O molecule as hydrogen acceptor. An HO···HOH type structure seems unlikely. It is well-known that hydrogen bond formation influences the IR spectrum, especially the OH stretching band of an OH···O hydrogen bond system, causing the band to shift to lower frequency, and becomes generally broader and stronger.[23] The observed intensity enhancement and frequency shift of the OH radical stretching band are consistent with hydrogen bond formation as mentioned above, while the bandwidth of the OH radical stretch of OH-H_2O does not become broader, but rather even sharper compared to the OH monomer.

Calculations. Figure 5 shows optimized structures of OH and OH-$(H_2O)_n$ ($n = 1-3$), calculated at the MP2 level of theory with an aug-cc-pVDZ basis set. Figure 6 shows optimized structures of $(H_2O)_n$ ($n = 1-4$), calculated in the same manner. The results are essentially as already reported.[24-27]

The OH-H_2O complex has an OH···OH_2 type structure, in good agreement with our result described above as well as results obtained by microwave spectroscopy and quantum chemical calculations.[6,8] The intermolecular distance $R_{O\cdots H}$ of OH···OH_2 is almost the same as $R_{HOH\cdots OH_2}$ of $(H_2O)_2$. Another local minimum on the OH-H_2O potential energy surface is located at the HO···HOH type structure, which is less stable than the OH···OH_2 type structure.[6,8] Table 3 lists binding energies, OH bond lengths, vibrational frequencies, and IR intensities for OH, H_2O, OH···OH_2, and HO···HOH. Unfortunately, the IR band corresponding to the HO···HOH complex was not observed in this study.

We also performed MP4(SDQ), B3LYP, and B98 calculations using various basis sets and obtained similar results. Table 4

TABLE 3: Binding Energies, OH Bond Lengths, Vibrational Frequencies, and IR Intensities for OH, H_2O, and OH-H_2O Isomers Calculated at the MP2/aug-cc-pVDZ Level of Theory

			H_2O bending		OH radical stretch	
	binding energy (cm^{-1})	OH bond lengths of OH radical (Å)	vibrational frequency (cm^{-1})	IR intensity (km/mol)	vibrational frequency (cm^{-1})	IR intensity (km/mol)
OH		0.97517			3768	16
H_2O			1622	68		
OH···OH_2	1770	0.98112	1622	67	3656	265
HO---HOH	1078	0.97650	1630	55	3751	34

TABLE 4: Rotational Constants, Vibrational Frequencies, and Frequency Shifts for OH-H_2O Calculated at Various Theoretical Levels Together with the Corresponding Experimental Values

		vibrational frequency of H_2O bending (cm^{-1})			vibrational frequency of OH radical stretch (cm^{-1})		
	rotational constant, $(B + C)/2$ (GHz)	OH-H_2O	H_2O monomer	shift	OH-H_2O	OH monomer	shift
B3LYP/aug-cc-pVDZ	6.78268	1615.1	1618.5	−3.4	3519	3681	−162
B3LYP/aug-cc-pVTZ	6.80168	1626.4	1627.5	−1.1	3535	3692	−157
B98/aug-cc-pVDZ	6.73003	1622.8	1626.3	−3.5	3567	3723	−156
B98/aug-cc-pVTZ	6.77923	1633.0	1635.8	−2.8	3578	3736	−156
MP2/aug-cc-pVDZ	6.46481	1622.0	1621.9	0.1	3655	3768	−113
MP2/aug-cc-pVTZ	6.65984	1629.9	1628.3	1.6	3668	3793	−125
MP4(SDQ)/aug-cc-pVDZ	6.37278	1645.5	1646.2	−0.7	3661	3734	−73
MP4(SDQ)/aug-cc-pVTZ	6.59432	1657.5	1657.2	0.3	3682	3768	−86
experimental data	6.57813[a]	1598.6[b]	1599.2[b]	−0.6[b]	3472.5[b]	3566[b]	−93.5[b]
					3452.2[c]	3549[c]	−96.8[c]

[a] Reference 8. [b] This work (Ne matrix). [c] Reference 6 (Ar matrix).

TABLE 5: Vibrational Frequencies of OH Radical Stretch, Frequency Shifts, IR Intensities, Binding Energies, and OH Bond Lengths for OH-$(H_2O)_n$ ($n = 0-3$) Complexes Calculated at the MP2/aug-cc-pVDZ Level of Theory

	OH	OH-H_2O	OH-$(H_2O)_2$	OH-$(H_2O)_3$
vibrational frequency of OH radical stretch (cm^{-1})	3768	3656	3548	3424
frequency shift upon complexation (cm^{-1})		−112	−220	−344
IR intensities (km/mol)	16	265	230	386
binding energy (D_e) (cm^{-1})		1770	4636	8169
OH bond length of OH radical (Å)	0.97517	0.98112	0.98696	0.99276

lists calculated rotational constants and vibrational frequencies for OH-H_2O, together with available experimental data. Frequencies for the OH radical stretch of OH-H_2O (Table 1) are red-shifted similarly to those for the OH monomer, although shift values are significantly scattered. Roughly speaking, DFT B3LYP and B98 calculations give lower vibrational frequencies than do MP2 and MP4 calculations, which reproduce experimental values well. MP2 and MP4 calculations give longer intermolecular distances between the O atom of H_2O and the H atom of OH, and shorter OH bond length, than do DFT calculations. MP2 and MP4 calculations give rotational constants for (B + C)/2 that reproduce experimental values well, while DFT calculations give larger values. MP2 and MP4 calculations give frequency shifts for the OH radical stretch of monomer to complex that are closer to the experimental than to DFT calculations. Thus, MP2 and MP4 are suitable for calculating OH-H_2O geometries, while DFT may overestimate intermolecular forces between OH and H_2O; therefore, the MP2 method with an aug-cc-pVDZ basis set was deemed sufficient to calculate values for larger complexes.

OH-$(H_2O)_2$ and OH-$(H_2O)_3$ complexes are likely to be ring-type structures, similar to the most stable structures of $(H_2O)_3$ and $(H_2O)_4$, respectively. Table 5 lists the calculated molecular

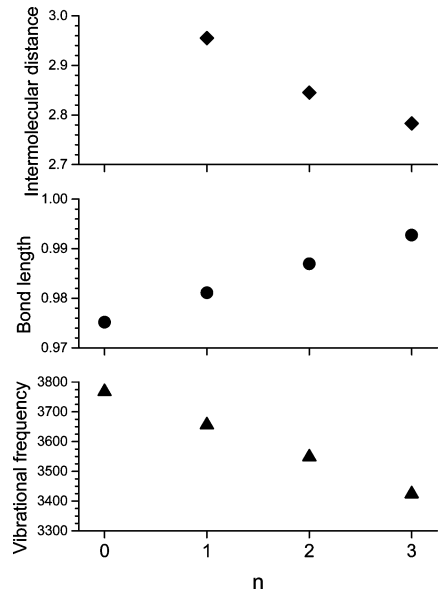

Figure 7. Plots of vibrational frequencies of OH radical stretch, O−H bond lengths, and intermolecular O−O distances of OH-$(H_2O)_n$ as a function of cluster size n.

parameters. Figure 7 shows plots of the vibrational frequencies of the OH radical stretch, bond lengths of the OH radical, and intermolecular distances estimated by the quantum chemical calculations as a function of the number of H_2O molecules n in the OH-$(H_2O)_n$ clusters. Distances in the figure are measured between the O atom of the OH radical, which is a donor, and the O atom of the H_2O molecule, which is an acceptor, in hydrogen bonding of OH···OH_2. The vibrational frequency and bond length of the OH radical show almost linear relationships with n. The intermolecular O−O distance of OH-$(H_2O)_n$ decreases with n, and approaches 2.7 Å with increasing n. These trends in molecular properties of OH-$(H_2O)_n$ are similar to the trends for water clusters reported in various experimental and theoretical studies. The bonded OH stretching vibrations in the

TABLE 6: Vibrational Frequencies and IR Intensities Calculated at Various Theoretical Levels Together with the Corresponding Experimental Values

	OH radical stretch of OH-H_2O			donor ν_1 of $(H_2O)_2$		
	frequency (cm^{-1})	IR intensity (km/mol)	freq gap (cm^{-1})	frequency (cm^{-1})	IR intensity (km/mol)	intensity ratio
B3LYP/aug-cc-pVDZ	3519.1	349.3	158.0	3677.1	321.4	1.09
B3LYP/aug-cc-pVTZ	3534.8	346.4	144.7	3679.5	331.4	1.05
B98/aug-cc-pVDZ	3566.9	324.8	154.4	3721.3	296.6	1.10
B98/aug-cc-pVTZ	3581.3	331.4	140.9	3722.2	309.1	1.07
MP2/aug-cc-pVDZ	3655.6	265.0	67.8	3723.4	226.2	1.17
MP2/aug-cc-pVTZ	3668.0	301.1	58.0	3726.0	272.5	1.11
MP4(SDQ)/aug-cc-pVDZ	3661.4	218.6	107.6	3769.0	178.5	1.22
experimental data	3472.5		118.0	3590.5		0.65

water cluster strongly correlate with cluster size.[16,20,28] The intermolecular O−O distance between adjacent H_2O's in a water cluster decreases exponentially with increasing cluster size.[26,27] These trends indicate that the hydrogen bonds become more linear, and stronger with increasing cluster size.[26] Hydrogen bond angles ∠O···H-O for the OH-$(H_2O)_2$ and OH-$(H_2O)_3$ clusters calculated in this study are 155° and 168°, respectively. Calculations predict that hydrogen bond strength within OH-$(H_2O)_n$ depends on cluster size, which probably correlates with cluster geometry.

Comparison of Observed Spectra and Calculations. The calculated red shift of the OH radical stretch of OH-$(H_2O)_2$ from the monomer OH is 219.5 cm^{-1}, twice the shift of OH-H_2O and close to the experimental value of −201 cm^{-1}. The calculated shift of OH-$(H_2O)_3$ from the unhydrated OH radical is −344 cm^{-1}, much larger than the experimental value of −201 cm^{-1}. Thus, we conclude that the band that is red-shifted by −201 cm^{-1} from the monomer OH band can be assigned to the OH radical stretch of OH-$(H_2O)_2$.

IR intensities of the OH radical stretch of OH-H_2O and the OH monomer exhibit unusual patterns as mentioned before; that is, the band due to OH-H_2O is much stronger than the band due to the OH monomer (Figure 2). Possible explanations are that their IR absorption coefficients and/or VUV photodissociation efficiencies are quite different. IR absorption coefficients for the OH radical stretch of OH-H_2O and the OH monomer were calculated by quantum chemical calculations (Table 4). Roughly speaking, all theories employed in this study show the coefficient for OH-H_2O to be much higher than that for the OH monomer, indicating that the coefficients contribute significantly to the very high ratio of OH-H_2O and OH monomer, while the role of quantum yields for photodissociation of OH-H_2O and OH monomer remains uncertain.

Consider now the IR band intensities of parent species $(H_2O)_2$ and product species OH-H_2O. In the OH stretching region, for VUV photodissociation, the product band is much stronger than the parent band (Figure 2); however, for dark reaction, depletion of the product band and production of the parent band are almost identical (Figure 3). In the H_2O bending region, the same trend is observed (Figure 4).

The fact that the dark reaction of OH-H_2O with an H atom occurs to form $(H_2O)_2$ indicates that there is an exact relationship between OH-H_2O depletion and $(H_2O)_2$ production. The fact that the OH-H_2O and $(H_2O)_2$ band intensities are comparable suggests that the IR absorption coefficient for the OH radical stretch in OH-H_2O is almost the same as for the OH stretch in $(H_2O)_2$. Quantum chemical calculations support this suggestion: the calculated absorption coefficient for the $(H_2O)_2$ band is 226 km/mol, comparable to that for the OH-H_2O band (Table 4). Abnormally weak depletion of $(H_2O)_2$ observed upon VUV photolysis suggests that VUV irradiation may induce production of $(H_2O)_2$, although the mechanism is uncertain. For higher water clusters, net production of $(H_2O)_n$ has been observed upon VUV irradiation (Table 2). These facts indicate that VUV irradiation induces the simultaneous and competing processes of photodissociation and cluster formation in the matrices.

Consider now, from a quantitative viewpoint, the ratio of IR band intensities for the OH radical stretch of OH-H_2O to donor ν_1 for $(H_2O)_2$ observed in the dark reaction (Figure 3). If loss of OH-H_2O converts directly to production of $(H_2O)_2$, the ratio of band intensities for OH-H_2O and $(H_2O)_2$ should be the same as the ratio of their calculated IR absorption coefficients. From experimental data (Figure 3), the ratio of integrated band intensities for the OH radical stretch of OH-H_2O to donor ν_1 for $(H_2O)_2$ is calculated to be 0.65. The IR absorption coefficients for the OH radical stretches of OH-H_2O and donor ν_1 for $(H_2O)_2$, calculated by various quantum chemical methods, are listed in Table 6. All calculations predict almost the same ratio of coefficients around 1.1, a bit larger than the experimental value of 0.65.

There are several possible reasons for this discrepancy. One possible reason is the accuracy of quantum chemical calculations. All calculation methods give roughly the same results for vibrational frequencies, while frequency gaps between OH radical stretch of OH-H_2O and donor ν_1 for $(H_2O)_2$ scatter extensively from 58 to 158 cm^{-1}. Moreover, the calculated IR absorption coefficients do not agree with each other. Thus, it might be necessary to use a quantum chemical calculation method with higher-order correlation correction, such as the CCSD(T) complete basis set limit, to reproduce the spectroscopic data in detail. A second possible reason might be the presence of another $(H_2O)_2$ source. Recombination of OH with a H atom to form H_2O is exothermic, and local heating effects may induce recombination of product of H_2O with a neighboring water molecule to form $(H_2O)_2$.

Conclusion

Hydrated hydroxyl radicals OH-$(H_2O)_n$ have been studied by FT-IR matrix isolation spectroscopy. Water clusters isolated in solid Ne were irradiated by 172 nm excimer lamp and photolyzed to form OH-$(H_2O)_n$. IR bands due to OH-$(H_2O)_n$ show a simple structure without any splitting due to site effects. IR bands due to the OH radical stretch and HOH bending vibrations of OH-H_2O and OH-$(H_2O)_2$ have been assigned with the aid of quantum chemical calculations. Reaction of OH-H_2O and H to form $(H_2O)_2$ observed under the dark conditions provides undisputed evidence for the spectroscopic assignments. Quantum chemical calculations predict the cyclic structure to be the most stable for OH-$(H_2O)_2$ and OH-$(H_2O)_3$. Relative IR intensities among reactants and products are discussed on the basis of reaction mechanisms and quantum chemical calculations.

References and Notes

(1) Hamad, S.; Lago, S.; Mejías, J. A. *J. Phys. Chem. A* **2002**, *106*, 9104.
(2) Cabral do Couto, P.; Guedes, R. C.; Costa Cabral, B. J. *J. Chem. Phys.* **2003**, *119*, 7344.
(3) Roeselová, M.; Vieceli, J.; Dang, L. X.; Garrett, B. C.; Tobias, D. J. *J. Am. Chem. Soc.* **2004**, *126*, 16308.
(4) Vieceli, J.; Roeselová, M.; Potter, N.; Dang, L. X.; Garrett, B. C.; Tobias, D. J. *J. Phys. Chem. B* **2005**, *109*, 15876.
(5) Langford, V. S.; McKinley, A. J.; Quickenden, T. I. *J. Am. Chem. Soc.* **2000**, *122*, 12859.
(6) Cooper, P. D.; Kjaergaard, H. G.; Langford, V. S.; McKinley, A. J.; Quickenden, T. I.; Schofield, D. P. *J. Am. Chem. Soc.* **2003**, *125*, 6048.
(7) Engdahl, A.; Karlstoröm, G.; Nelander, B. *J. Chem. Phys.* **2003**, *118*, 7797.
(8) Ohshima, Y.; Sato, K.; Sumiyoshi, Y.; Endo, Y. *J. Am. Chem. Soc.* **2005**, *127*, 1108.
(9) Tsuge, M.; Tsuji, K.; Kawai, A.; Shibuya, K. *J. Phys. Chem. A* **2007**, *111*, 3540.
(10) Frisch, M. J.; Trucks, G. W.; Schlegel, H. B.; Scuseria, G. E.; Robb, M. A.; Cheeseman, J. R.; Montgomery, J. A., Jr.; Vreven, T.; Kudin, K. N.; Burant, J. C.; Millam, J. M.; Iyengar, S. S.; Tomasi, J.; Barone, V.; Mennucci, B.; Cossi, M.; Scalmani, G.; Rega, N.; Petersson, G. A.; Nakatsuji, H.; Hada, M.; Ehara, M.; Toyota, K.; Fukuda, R.; Hasegawa, J.; Ishida, M.; Nakajima, T.; Honda, Y.; Kitao, O.; Nakai, H.; Klene, M.; Li, X.; Knox, J. E.; Hratchian, H. P.; Cross, J. B.; Bakken, V.; Adamo, C.; Jaramillo, J.; Gomperts, R.; Stratmann, R. E.; Yazyev, O.; Austin, A. J.; Cammi, R.; Pomelli, C.; Ochterski, J. W.; Ayala, P. Y.; Morokuma, K.; Voth, G. A.; Salvador, P.; Dannenberg, J. J.; Zakrzewski, V. G.; Dapprich, S.; Daniels, A. D.; Strain, M. C.; Farkas, O.; Malick, D. K.; Rabuck, A. D.; Raghavachari, K.; Foresman, J. B.; Ortiz, J. V.; Cui, Q.; Baboul, A. G.; Clifford, S.; Cioslowski, J.; Stefanov, B. B.; Liu, G.; Liashenko, A.; Piskorz, P.; Komaromi, I.; Martin, R. L.; Fox, D. J.; Keith, T.; Al-Laham, M. A.; Peng, C. Y.; Nanayakkara, A.; Challacombe, M.; Gill, P. M. W.; Johnson, B.; Chen, W.; Wong, M. W.; Gonzalez, C.; Pople, J. A. *Gaussian 03*, revision C.02; Gaussian, Inc.: Wallingford, CT, 2004.
(11) Boys, S. F.; Bernardi, F. *Mol. Phys.* **1970**, *19*, 553.
(12) Suenaga, M. *J. Comput. Chem. Jpn.* **2005**, *4*, 25–32.
(13) Suenaga, M. *J. Comput. Chem. Jpn.* **2008**, *7*, 33–53.
(14) Forney, D.; Jacox, M. E.; Thompson, W. E. *J. Mol. Spectrosc.* **1993**, *157*, 479.
(15) Bouteiller, Y.; Perchard, J. P. *Phys. Chem.* **2004**, *305*, 1.
(16) Paul, J. B.; Collier, C. P.; Saykally, R. J.; Scherer, J. J.; O'Keefe, A. *J. Phys. Chem. A* **1997**, *101*, 5211.
(17) Bentwood, R. M.; Barnes, A. J.; Orville-Thomas, W. J. *J. Mol. Spectrosc.* **1980**, *84*, 391.
(18) Engdahl, A.; Nelander, B. *J. Mol. Struct.* **1989**, *193*, 101.
(19) Perchard, J. P. *Chem. Phys.* **2001**, *273*, 217.
(20) Hirabayashi, S.; Yamada, K. M. T. *J. Chem. Phys.* **2005**, *122*, 244501.
(21) Eberlein, J.; Creuzburg, M. *J. Chem. Phys.* **1997**, *106*, 2188.
(22) Vaskonen, K.; Eloranta, J.; Kiljunen, T.; Kunttu, H. *J. Chem. Phys.* **1999**, *110*, 2122.
(23) Pimentel, G. C.; McClellan, A. L. Methods of Detection: Infrared and Raman Spectroscopy. *The Hydrogen Bond*; W. H. Freeman and Company: San Francisco, 1960; pp 67−102.
(24) Gregory, J. K.; Clary, D. C. *J. Phys. Chem.* **1996**, *100*, 18014.
(25) Xantheas, S. S.; Burnham, C. J.; Harrison, R. J. *J. Chem. Phys.* **2002**, *116*, 1493.
(26) Xantheas, S. S.; Dunning, T. H., Jr. *J. Chem. Phys.* **1993**, *99*, 8774.
(27) Lee, H. M.; Suh, S. B.; Lee, J. Y.; Tarakeshwar, P.; Kim, K. S. *J. Chem. Phys.* **2000**, *112*, 9759.
(28) Buck, U.; Huisken, F. *Chem. Rev.* **2000**, *100*, 3863.

JP903648Z